Nanoscale Research Letters

NANO EXPRESS

Open Access

Red Light-Emitting Diodes with All-Inorganic $CsPbI_3$/TOPO Composite Nanowires Color Conversion Films

Lung-Chien Chen[1*], Yi-Tsung Chang[2†], Ching-Ho Tien[1†], Yu-Chun Yeh[1], Zong-Liang Tseng[3], Kuan-Lin Lee[2] and Hao-Chung Kuo[4]

Abstract

This work presents a method for obtaining a color-converted red light source through a combination of a blue GaN light-emitting diode and a red fluorescent color conversion film of a perovskite $CsPbI_3$/TOPO composite. High-quality $CsPbI_3$ quantum dots (QDs) were prepared using the hot-injection method. The colloidal QD solutions were mixed with different ratios of trioctylphosphine oxide (TOPO) to form nanowires. The color conversion films prepared by the mixed ultraviolet resin and colloidal solutions were coated on blue LEDs. The optical and electrical properties of the devices were measured and analyzed at an injection current of 50 mA; it was observed that the strongest red light intensity was 93.1 cd/m^2 and the external quantum efficiency was 5.7% at a wavelength of approximately 708 nm when $CsPbI_3$/TOPO was 1:0.35.

Keywords: Perovskite quantum dot, $CsPbI_3$, Color conversion film, Trioctylphosphine oxide

Background

Numerous types of quantum dots (QDs), including CdSe QDs [1], carbon QDs [2], InP QDs [3], $CuInS_2$ QDs [4], CdTe QDs [5], and perovskite QDs [6, 7], were widely studied to be involved in the main mechanism that underlies the observed phenomenon. QDs have been utilized in the field of light-emitting diodes (LEDs) [8, 9], solar cells [10, 11], photodetectors [12, 13], and biomarkers [14, 15] and have been adopted to construct sensors to detect biologically interesting molecules [16]. In particular, a perovskite material was the most popular potential materials in recent years, and enormous progress and applications have been made in this direction [17–23]. They can be synthesized to have various dimensional morphologies, including three-dimensional (3D) morphologies such as thin film and bulk single crystal, two-dimensional (2D) morphologies such as nanoplates and nanosheets, one-dimensional (1D) such as nanowires and nanorods, and zero-dimensional (0D) morphologies such as QDs and nanoparticle structures. All-inorganic perovskite QDs ($CsPbX_3$, X = Cl, Br, I) have excellent optical properties such as a high absorption coefficient, a narrow half-peak width of 20–40 nm, a quantum yield of up to 90%, and higher stability than hybrid organic–inorganic perovskite QDs [such as $MAPbX_3$ and $FAPbX_3$ (X = Cl, Br, I)] [24–27]. The synthesis method is simple and low cost and is expected to replace traditional fluorescent materials. Moreover, by adjusting the ratio of halogen element X (X = Cl, Br, I), we can adjust the emission wavelength of perovskite $CsPbX_3$ QDs from 380 to 780 nm and can achieve an all-visible light region [28–30]. The integration of perovskite QDs into LEDs can achieve a breakthrough of more than 110% of the NTSC color gamut and a better color rendering performance [23, 31–34]. This showed that $CsPbI_3$ QD has considerable potential to become a candidate material for red

*Correspondence: ocean@ntut.edu.tw
†Yi-Tsung Chang and Ching-Ho Tien have contributed equally to this work
[1] Department of Physics, School of Science, JiMei University, Xiamen 361021, China
Full list of author information is available at the end of the article

phosphor. In contrast, cadmium-containing QDs were highly toxic. After they were prepared into various types of application-end products, the environmental damage was considerable. Considering environmental protection issues, the development of cadmium-free QD materials is necessary, but the efficiency of cadmium-free materials is poor, the full width at half maximum (FWHM) is wide, the improvement in efficiency and the control of FWHM are the focus of the development of cadmium-free QDs, and the instability of perovskite-based devices still hinders their entry to the commercial market [35]. As far as we know, there have been few reports on the use of $CsPbI_3$ QDs as red phosphor to manufacture red LEDs, most of which include the addition of the halogen element Br to form $CsPbBr_xI_{3-x}$ QDs [36–38].

Trioctylphosphine oxide (TOPO), a highly branched capping ligand with a strong steric effect, is commonly used as a capping ligand for conventional II–VI, III–V, and IV–VI QDs [39–41]. Because of the highly branched molecular structure and the relatively strong coordination ability of the P=O group, TOPO species can cooperate with the surface of the obtained QDs through a certain scheme, thereby providing a more complete surface passivation for the QDs [42–44]. Zhang and co-workers successfully synthesized the monodisperse TOPO-capped $CsPbX_3$ QDs with excellent stability against an ethanol solvent attack by introducing TOPO in the Pb precursor with an oleic acid (OA) and oleylamine (OAm) system [45]. Zhang et al. [46] performed a novel synthesis of $CsPb_xMn_{1-x}Cl_3$ QDs by using TOPO and a Mn organometallic complex as the Mn reaction precursor, which exhibited PLQYs as high as 63% and excellent dispersibility and stability. Herein, we present a hot-injection method to synthesize $CsPbI_3$ QDs and then prepare a perovskite $CsPbI_3$/TOPO composite with high PL intensity by introducing TOPO into the $CsPbI_3$ QD solution. We found that the $CsPbI_3$/TOPO composite could form $CsPbI_3$ nanowires and QDs, as well as show excellent material and optical characteristics. Then, the $CsPbI_3$/TOPO composite was uniformly mixed with UV resin to prepare a color conversion fluorescent film, and a color-converted pure red LED was obtained by exciting the blue GaN-based LED chip.

Methods

Cesium carbonate (Cs_2CO_3, 99.998%) and lead (II) iodide (PbI_2, 99.999%) were purchased from Alfa Aesar. 1-octadecene (ODE, 90%), oleic acid (OA, 90%), oleylamine (OAM, 90%), and trioctylphosphine oxide (TOPO, 99%) were purchased from Sigma-Aldrich. Ethyl acetate (EA), n-hexane, and acetone were purchased from Echo Chemical. Ultraviolet (UV) resin (U-76063S-A) was purchased from Synergy Innovation.

Perovskite $CsPbI_3$ QDs were prepared by using the hot-injection and ice water bath methods, as presented in Fig. 1. Firstly, 81.4 mg of Cs_2CO_3 and 0.25 mL of OA were added to a glass vial containing 3 mL of ODE, and the mixture was placed on a 200 °C hot plate and stirred magnetically for 0.5 h until completely dissolved to form an optically clear Cs-oleate precursor solution. Then, PbI_2 (200 mg), OA (1 mL), and OAm (1 mL) were added to a glass bottle containing ODE (10 mL), and the mixture was placed in a 140 °C heating bag and stirred for 0.5 h until the PbI_2 salt had completely dissolved. Thereafter, the heating temperature was increased to 160 °C and stirred for 5 min, followed by quickly injecting 0.8 mL of the Cs-oleate precursor solution by using a micro-dropper. After 10 s, the $CsPbI_3$ crude solution was placed in an ice water bath for 40 s to immediately stop the reaction and was cooled to room temperature. To wash the $CsPbI_3$ QDs, the crude solution was precipitated by using the EA washing solvent in a volume ratio of 1:4 via centrifugation with 6000 rpm for 15 min and finally dispersed in 1 mL of n-hexane under ultrasonication for further use. All the synthesis and washing occurred under ambient atmospheric conditions.

Furthermore, 20 mg of TOPO powders was added into 1 mL of hexane and at room temperature while stirring at 600 rpm until the powders were completely dissolved. Subsequently, the perovskite $CsPbI_3$ QD solution was added to the TOPO/hexane system with different volume ratios (volume ratios 1:0.15, 1:0.35, and 1:0.60 of $CsPbI_3$ QDs and TOPO) while stirring for 1 min at room temperature to obtain the $CsPbI_3$/TOPO composites.

The different ratios of $CsPbI_3$/TOPO composites were mixed with the UV resin (volume ratio 1:2 of $CsPbI_3$/TOPO composite and UV resin). Then, the resulting mixture was vacuumed for 0.5 h to remove the bubbles. The different ratios of $CsPbI_3$/TOPO–UV resins were obtained. The blue GaN-based LED chip (1 mm × 1 mm) with an emission wavelength of 455 nm was mounted in a groove with a diameter of approximately 7 mm. Thereafter, these mixtures were coated/filled onto glass substrates and blue LED chips and baked at 40 °C for 3 min and then cured using a 365 nm UV lamp for 60 s in the glove box to form color conversion films and color-converted red LEDs, as shown in Fig. 2.

For the characterization, the crystal phases, absorption spectrum, photoluminescence (PL) spectra, and PL quantum yield (PLQY) of $CsPbI_3$ QDs and $CsPbI_3$/TOPO composites were obtained using field-emission scanning electron microscope (FESEM) (ZEISS Sigma, ZEISS, Munich, Germany), high-resolution transmission electron microscopy (HRTEM) (JEM-2100F, JEOL, Tokyo, Japan), X-ray diffraction (XRD) with CuKα radiation (X'Pert PRO MRD, PANalytical, Almelo, The

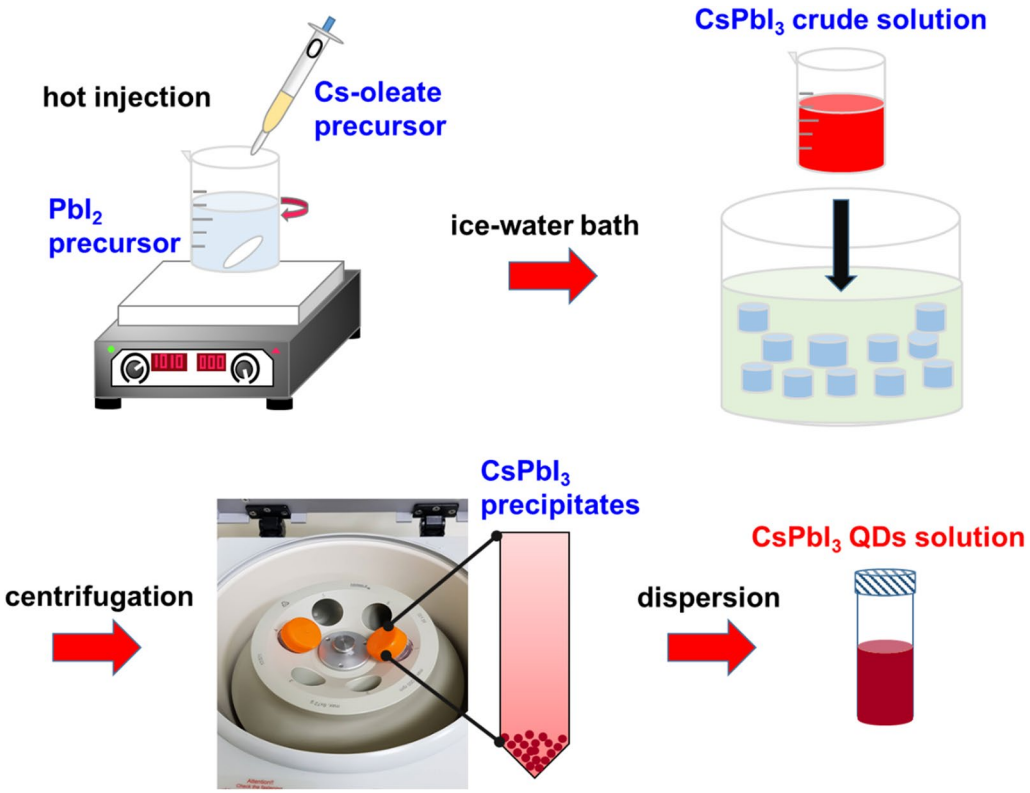

Fig. 1 Schematic representation of the synthesis of perovskite $CsPbI_3$ QDs via hot-injection and ice water bath methods

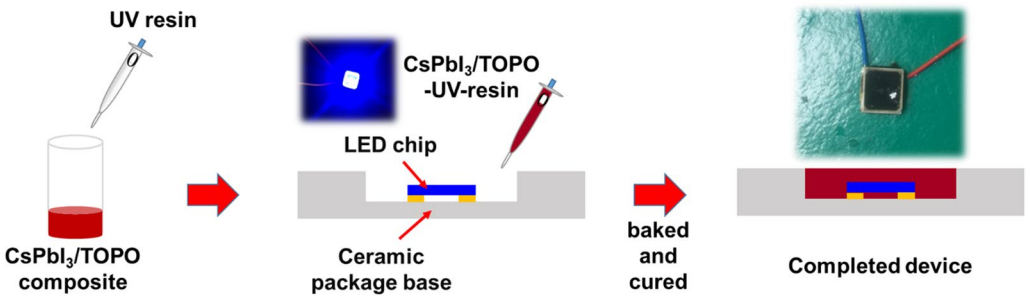

Fig. 2 Schematic representation of encapsulating strategy

Netherlands), UV–Vis spectrophotometer (Thermo Scientific™ Evolution 220, Thermo Fisher Scientific, Taiwan), fluorescence spectrophotometer (F-7000, Hitachi, Tokyo, Japan), and a FluoroMax spectrofluorometer with an integrating sphere fiber coupled to a fluorometer (Horiba Jobin Yvon, Longjumeau, France). The current–voltage (I–V), luminance, external quantum efficiency (EQE) characteristics, and electroluminescence (EL) spectra of perovskite color-converted red LEDs were measured by a Keithley 2400 source meter and a Spectrascan® spectroradiometer PR-670 (Photo Research Inc., Syracuse, NY, USA) at room temperature.

Results and Discussion

The crystal structures of the obtained $CsPbI_3$/TOPO composite films with different ratios were characterized by using XRD, as shown in Fig. 3. The addition of TOPO did not change the microscopic reorganization of $CsPbI_3$ QDs, and the QDs were located at approximately 14.95° and 29.1°, corresponding to the (100) and (200) crystal planes of the $CsPbI_3$ cubic lattice structure,

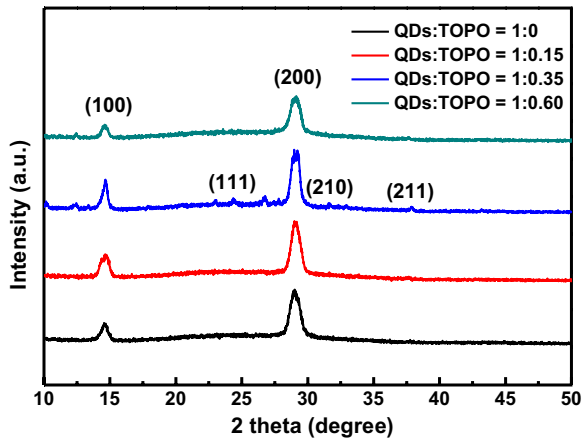

Fig. 3 X-ray diffraction (XRD) patterns of $CsPbI_3$/TOPO composite films with different ratios

respectively. Moreover, no crystal binding or by-products appeared with other small crystal diffraction peaks. When the $CsPbI_3$/TOPO ratio was 1:0.35, the diffraction peak of the perovskite $CsPbI_3$/TOPO composite film in the XRD pattern was stronger and sharper than that of the other $CsPbI_3$/TOPO ratios; meanwhile, the (111), (210), and (211) crystal planes of other cubic lattice structures appeared, which confirmed that the perovskite composite prepared with this parameter had better crystallinity [47, 48]. In contrast, excessive TOPO ($CsPbI_3$/TOPO = 1:0.60) led to a decrease in perovskite crystallinity, which could be attributed to the excessive amount of TOPO that caused the $CsPbI_3$ QDs to produce more nanowire-like structures, resulting in a decrease in film compactness.

Figure 4 shows the film formation SEM images of $CsPbI_3$/TOPO composite films with different ratios coated on the glass substrates. Figure 4a shows the morphology of the $CsPbI_3$ QD film without TOPO, which was formed by the aggregation of discontinuous, large grains and QDs. After the addition of different ratios of TOPO, surprisingly, the nanowires of the $CsPbI_3$/TOPO composite films with diameters of 50–160 nm and lengths up to several microns, as well as QDs adhered to the nanowires, were observed (Fig. 4b–d). In addition, when the amount of TOPO increased, most of the $CsPbI_3$/TOPO composite materials formed thicker nanowires and the QD grain size increased, resulting in reduced film coverage and poor quality.

According to the XRD and SEM results, nanowires and QDs can be obtained by adding TOPO to the

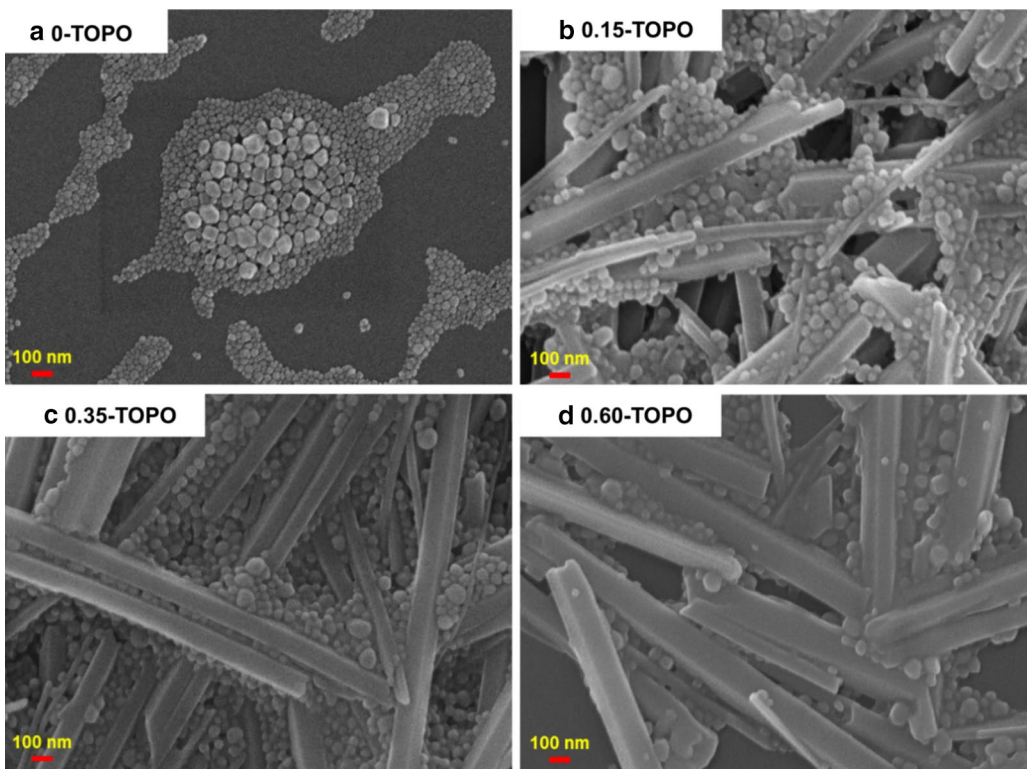

Fig. 4 Top view of SEM micrographs of $CsPbI_3$/TOPO composite films with different ratios: **a** 1:0, **b** 1: 0.15, **c** 1:0.35, **d** 1:0.60

$CsPbI_3$ QD solution. We chose to have better $CsPbI_3$/TOPO composite ($CsPbI_3$/TOPO = 1:0.35) quality and analyze its nanowires and QDs by using HRTEM. The HRTEM images of the perovskite $CsPbI_3$ QDs and the $CsPbI_3$/TOPO composite ($CsPbI_3$/TOPO = 1:0.35) solutions are displayed in Fig. 5a, b. Figure 5a clearly shows that TOPO-free $CsPbI_3$ had a cubic shape and uniformly arranged QDs and was measured to have a narrow size distribution in the range of 7–12 nm. $CsPbI_3$ nanowires and QDs were obtained when the ratio was $CsPbI_3$/TOPO = 1:0.35, as shown in Fig. 5b. The nanowires of the $CsPbI_3$/TOPO composite were in a broad diameter range of 7–14 nm with a length range of 50–170 nm, and the particle size range of QDs was 5–8 nm (Fig. 5c). We attributed the formation of the nanowire-type structure to the coordination bonds between the O-donor base in TOPO (Lewis base) and the perovskite QDs. It was attributed to the fact that the Pb in the $CsPbI_3$ was a Lewis acid and TOPO was a Lewis base. In the Lewis acid–base interactions, a base was defined as the electron donors and an acid was defined as the electron acceptors. A Lewis acid–base reaction occurred when a base donated a pair of electrons to an acid, which formed a Lewis acid–base adduct, a compound that contained a coordinate covalent bond between the Lewis acid and the Lewis base [30, 47]. An energy-dispersive X-ray (EDX) analysis was performed to check the composition and the stoichiometric ratio of the nanowires in the $CsPbI_3$/TOPO composite, and the result is shown in Fig. 5d. There were no impurity element-related peaks in the EDX spectrum, which confirmed the XRD result of the pure phase formation. The observed constituent elements and atomic ratios were proved to be $CsPbI_3$. In addition, we found that the size of the nanowires and QDs as observed by TEM was different from that obtained from the SEM analysis, which might be attributed to the aggregation phenomenon caused by the solution after spin coating.

Figure 6 compares the effects of different TOPO ratios on the UV–Vis absorption and PL spectra of the perovskite $CsPbI_3$/TOPO composite films, where the absorption peak was at approximately 700 nm, while the PL peak was located at approximately 692 nm. Table 1 shows the optical properties of $CsPbI_3$ QDs and $CsPbI_3$/TOPO composite films. Figure 6a shows that the TOPO treatment caused a slight shift in absorption; it was observed that the absorption of the $CsPbI_3$/TOPO composite film enhanced slightly as the TOPO content increased. However, the absorption slightly declined when the ratio of $CsPbI_3$/TOPO exceeded 1:0.35. In the visible-light region (470–800 nm), the absorbance of the $CsPbI_3$/TOPO composite film prepared with the $CsPbI_3$/TOPO ratio of 1:0.35 increased, indicating improved crystallinity.

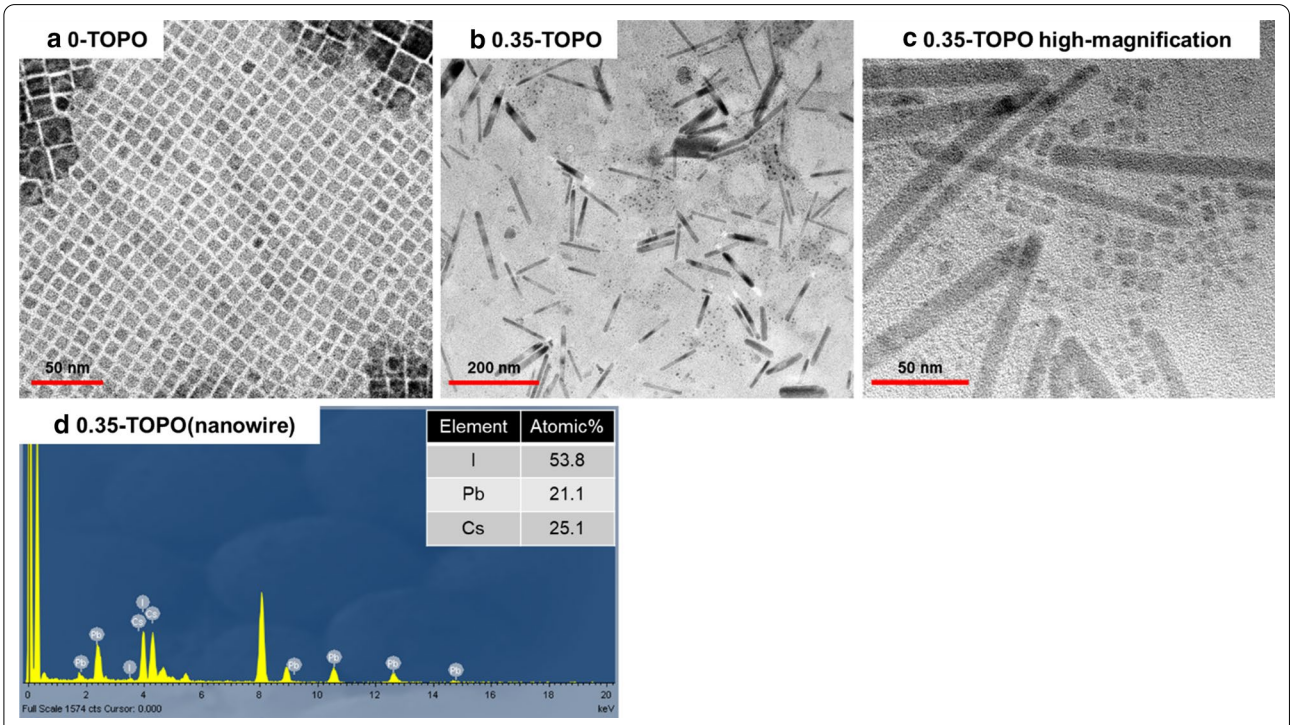

Fig. 5 High-resolution TEM (HRTEM) micrographs of $CsPbI_3$/TOPO composite solutions with different ratios: **a** 1:0, **b** 1:0.35, **c** 1:0.35 high-magnification, **d** energy-dispersive X-ray (EDX) analysis for the nanowire in the $CsPbI_3$/TOPO composite

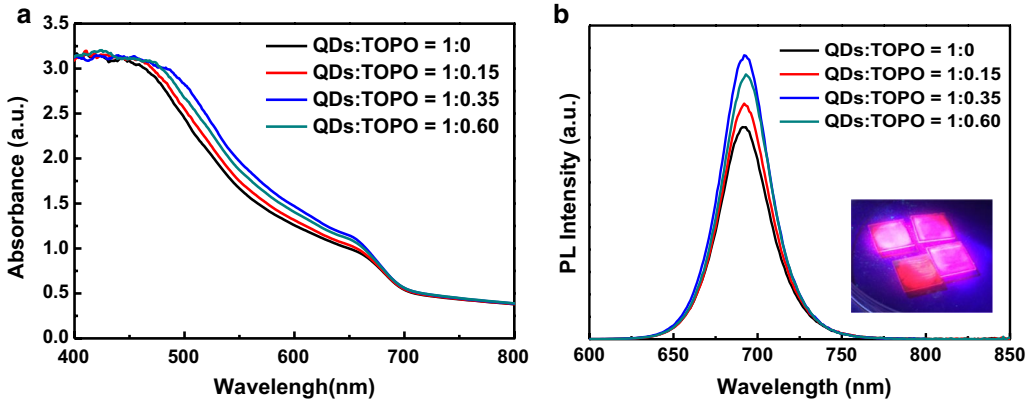

Fig. 6 **a** Ultraviolet–visible (UV–Vis) absorption spectra, **b** photoluminescence (PL) spectra of $CsPbI_3$/TOPO composite films with different ratios; the inset is the fluorescence photograph of the $CsPbI_3$/TOPO composites/glass under 365 nm light excitation

Table 1 Optical properties of $CsPbI_3$ QDs and $CsPbI_3$/TOPO composite films

QDs/TOPO	1:0	1:0.15	1:0.35	1:0.60
PL (nm)	691	692	692	693
FWHM (nm)	37.9	37.2	36.4	36.8
PLQY (%)	32.8	35.8	47.2	37.4

Figure 6b shows the observation that the PL intensity of all perovskite $CsPbI_3$/TOPO composite films added with TOPO was higher than that of the $CsPbI_3$ QD film without TOPO. When UV light was irradiated on the perovskite $CsPbI_3$/TOPO composite films, the films absorbed the photons and caused the electrons in the valence band to jump to the conduction band. The photons in the conduction band transitioned back to the valence band for emission or to fall into the traps in the film to be quenched. Therefore, when the perovskite $CsPbI_3$/TOPO composite films had high quality and relatively few traps or defects, the fluorescent signal was stronger. When the $CsPbI_3$/TOPO ratio was 1:0.35, the PL intensity was the strongest with a high PLQY of 47.2% and a narrow FWHM of approximately 36.4 nm, which implied that the perovskite $CsPbI_3$/TOPO composite film prepared in this ratio was of high quality.

As presented in Fig. 7a, the I–V curves of the $CsPbI_3$/TOPO composite-converted red LEDs with different ratios were almost the same, confirming that the coating QDs had nearly no influence on the LED circuit. The luminance–current (L–I) and EQE–current (EQE–I) characteristics for all the LED devices are shown in Fig. 7b, c, and the optoelectronic characteristics of the devices are summarized in Table 2. We found that the maximum brightness and EQE values of the devices increased first and then slightly declined with a continuous increase in the TOPO content of the $CsPbI_3$/TOPO composite. The performances of the $CsPbI_3$/TOPO composite-converted red LEDs could be optimized by altering the TOPO amount, and the optimized ratio of $CsPbI_3$/TOPO was 1:0.35. The optimized $CsPbI_3$/TOPO composite-converted red LED device exhibited a turn-on voltage of 2.65 V (@20 mA) and maximum brightness and EQE values of 93.1 cd/m^2 and 5.7%, respectively, which were significantly better than those of the other devices. In contrast, the maximum brightness and EQE values of the other $CsPbI_3$/TOPO ratios (1:0, 1:0.15, and 1:0.60) were 57.1, 66.5, and 44.8 cd/m^2, as well as 3.0%, 4.0%, and 2.4%, respectively. However, the surface defects caused by the $CsPbI_3$/TOPO composite films treated with excessive TOPO content reduced the ability of fluorescence conversion, resulting in a significant decrease in both luminance and EQE. This result was inferred from the SEM observation that excessive TOPO content led to a decrease in the film coverage and quality. The emission spectra of all the $CsPbI_3$/TOPO composite-converted red LEDs with different ratios under a driving current of 50 mA are shown in Fig. 7d, which illustrates that all the color-converted devices had a major EL peak at 708 nm with a FWHM of approximately 34 nm.

We found that the luminance of a $CsPbI_3$/TOPO composite-converted red LED dropped by only 31.42%, whereas it dropped by up to 75.68% for a $CsPbI_3$-converted red LED, as shown in Fig. 8. The luminance of a $CsPbI_3$-converted red LED showed a rapid linear decrease with an increase in the stored time, while a $CsPbI_3$/TOPO-converted red LED showed that ~85% of the initial value was maintained even within the first four days. Thus, we concluded that a $CsPbI_3$/TOPO-converted red LED not only had more luminance than

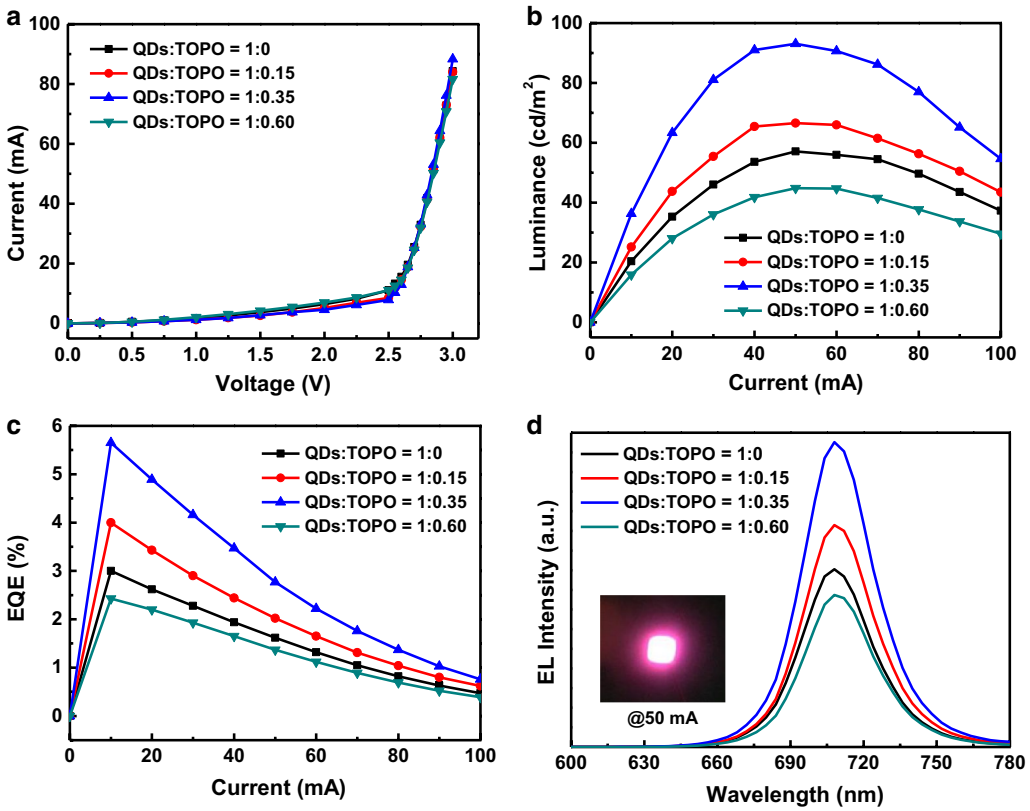

Fig. 7 Performances of $CsPbI_3$/TOPO composite-converted red LEDs under different driving current. **a** I–V, **b** L–I, **c** EQE–I curves, **d** EL spectra. The inset is an optical photograph of a color-converted red LED at 50 mA

Table 2 Optoelectronic properties of $CsPbI_3$/TOPO composite-converted red LEDs

QDs/TOPO	1:0	1:0.15	1:0.35	1:0.60
L_{max} (cd/m^2)	57.1	66.5	93.1	44.8
EQE_{max} (%)	3.0	4.0	5.7	2.4

the $CsPbI_3$-converted design but also improved stability. Although a $CsPbI_3$/TOPO composite material is proposed to incorporate TOPO to improve the quality of the quantum-sized composite material, the stability of the composite material still needs to be improved to meet the practical application standards in future work.

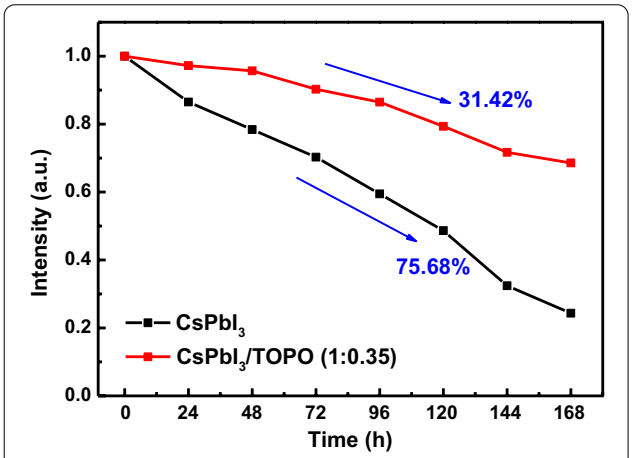

Fig. 8 Stability of $CsPbI_3$-converted and $CsPbI_3$/TOPO composite-converted red LEDs

Conclusions

In conclusion, we presented a simple method to prepare all-inorganic perovskite $CsPbI_3$ QDs under ambient atmosphere and then combined a TOPO solution to obtain the $CsPbI_3$/TOPO composite including QDs and NWs. The TEM image was obtained; it revealed that the perovskite $CsPbI_3$ gradually changed from a QD type to a nanowire type with an increase in the amount of TOPO. The PL spectra were examined. They revealed that the PL intensity of $CsPbI_3$/TOPO composites increased with increasing TOPO; the PLQY of the

$CsPbI_3$/TOPO composite also improved as compared to that of the TOPO-free $CsPbI_3$ QDs. Finally, it was applied in a color conversion device using the UV resin; it could be easily made into a quantum composite thin film and affected by water and oxygen, thereby extending the lifetime of the $CsPbI_3$/TOPO composite in the atmospheric environment.

Abbreviations

$CsPbI_3$: Cesium lead tri-iodide; Cs_2CO_3: Cesium carbonate; PbI_2: Lead iodide; ODE: Octadecene; OA: Oleic acid; OAM: Oleylamine; EA: Ethyl acetate; TOPO: Trioctylphosphine oxide; QDs: Quantum dots; LED: Light-emitting diode.

Acknowledgements

This work was supported by the Ministry of Science and Technology (Taiwan) under Contract Nos. 108-2221-E-027-093, 108-2221-E-131-009-MY2, and 109-2218-E-027-003-MY2.

Authors' Contributions

L-CC carried out the experiments and designed the study and gave significant suggestions on writing the whole manuscript. Y-TC and C-HT conceived the original idea and wrote the manuscript. Y-CY and K-LL prepared the samples and performed all measurements. Z-LT and H-CK helped to analyze and interpret the data and helped to draft the manuscript. All authors read and approved the final manuscript.

Funding

This work was supported by the Ministry of Science and Technology (Taiwan) under Contract Nos. 108-2221-E-027-093, 108-2221-E-131-009-MY2, and 109-2218-E-027-003-MY2.

Availability of Data and Materials

All the data are fully available without restrictions.

Ethics Approval and Consent to Participate

Not applicable.

Competing interests

The authors declare that they have no competing interests.

Author details

[1] Department of Physics, School of Science, JiMei University, Xiamen 361021, China. [2] Department of Electro-Optical Engineering, National Taipei University of Technology, Taipei 10608, Taiwan. [3] Department of Electronic Engineering, Ming Chi University of Technology, New Taipei City 24301, Taiwan. [4] Department of Photonics and Institute of Electro-Optical Engineering, National Chiao Tung University, Hsinchu 30010, Taiwan.

Received: 24 July 2020 Accepted: 8 October 2020
Published online: 16 November 2020

References

1. Cheng R, Li F, Zhang J, She X, Zhang Y, Shao K, Lin Y, Wang CF, Chen S (2019) Fabrication of amphiphilic quantum dots towards high-colour-quality light-emitting devices. J Mater Chem C 7(14):4244–4249. https://doi.org/10.1039/C9TC00113A
2. Lin H, Yang J, Liu YF, Zeng FJ, Tang XS, Yao ZQ, Guan HL, Xiong Q, Zhou JE, Wu DF, Du J (2020) Stable and efficient hybrid Ag–In-S/ZnS@SiO_2-carbon quantum dots nanocomposites for white light-emitting diodes. Chem Eng J 393:124654. https://doi.org/10.1016/j.cej.2020.124654
3. Wang L, Lin J, Liu X, Cao S, Wang Y, Zhao J, Zou B (2020) Mg doped-ZnO nanoparticle film as the interlayer between ZnO electron transport layer and InP quantum-dot layer for light-emitting diodes. J Phys Chem C 124(20):11274. https://doi.org/10.1021/acs.jpcc.0c03868
4. Wang T, Guan X, Zhang H, Ji W (2019) Exploring electronic and excitonic processes toward efficient deep-red $CuInS_2$/ZnS quantum-dot light-emitting diodes. ACS Appl Mater Interfaces 11(40):36925–36930. https://doi.org/10.1021/acsami.9b13108
5. Zhang X, Sun Z, Zhou C, Zhu Z, Guo Z, Shen J, Lin Yu, Xiao S, Chen L, Zheng X, Wu ZC (2019) Synthesis and enhanced photo/thermal stability of high-luminescent red-emitting CdTe@CaCO3 composite for LED applications. Ceram Int 45(5):6484–6490. https://doi.org/10.1016/j.ceramint.2018.12.137
6. Wang Y, Zhang R, Yue Y, Yan S, Zhang L, Chen D (2020) Room temperature synthesis of CsPbX3 (X = Cl, Br, I) perovskite quantum dots by water-induced surface crystallization of glass. J Alloys Compd 818:152872. https://doi.org/10.1016/j.jallcom.2019.152872
7. Yang B, Zheng F, Mei S, Chen Z, Xie Y, Dai H, Wei X, Zhang W, Xie F, Ju J, Chu Y, Zou J, Guo R (2020) Component regulation and crystallization mechanism of $CsPbBr_3$/$Cs4PbBr_6$ perovskite composite quantum dots-embedded borosilicate glass for light emitting application. Appl Surf Sci 512:145655. https://doi.org/10.1016/j.jallcom.2019.152872
8. Khan Q, Subramanian A, Yu G, Maaz K, Li D, Sagar RUR, Chen K, Lei W, Shabbir B, Zhang Y (2019) Structure optimization of perovskite quantum dot light-emitting diodes. Nanoscale 11(11):5021–5029. https://doi.org/10.1039/c8nr09864f
9. Xiang C, Wu L, Lu Z, Li M, Wen Y, Yang Y, Liu W, Zhang T, Cao W, Tsang SW, Shan B, Yan X, Qian L (2020) High efficiency and stability of ink-jet printed quantum dot light emitting diodes. Nat Commun 11:1646. https://doi.org/10.1038/s41467-020-15481-9
10. Zhou F, Li Z, Chen H, Wang Q, Ding L, Jin Z (2020) Application of perovskite nanocrystals (NCs)/quantum dots (QDs) in solar cells. Nano Energy 73:104757. https://doi.org/10.1016/j.nanoen.2020.104757
11. Jia D, Chen J, Yu M, Liu J, Johansson EMJ, Hagfeldt A, Zhang X (2020) Dual passivation of $CsPbI_3$ perovskite nanocrystals with amino acid ligands for efficient quantum dot solar cells. Small 16(24):2001772. https://doi.org/10.1002/smll.202001772
12. Bi CH, Kershaw SV, Rogach AL, Tian JJ (2019) Improved stability and photodetector performance of $CsPbI_3$ perovskite quantum dots by ligand exchange with aminoethanethiol. Adv Funct Mater 29(29):1902446. https://doi.org/10.1002/adfm.201902446
13. Li JZ, Xia JM, Liu Y, Zhang SW, Teng CJ, Zhang X, Liu BL, Zhao SC, Zhao SX, Li BH, Xing GC, Kang FY, Wei GD (2019) Ultrasensitive organic-modulated $CsPbBr_3$ quantum dot photodetectors via fast interfacial charge transfer. Adv Mater Interfaces 7(2):1901741. https://doi.org/10.1002/admi.201901741
14. Yezhelyev MV, Al-Hajj A, Morris C, Marcus AI, Liu T, Lewis M, Cohen C, Zrazhevskiy P, Simons JW, Rogatko A, Nie S, Gao X, O'Regan RM (2007) In situ molecular profiling of breast cancer biomarkers with multicolor quantum dots. Adv Mater 19(20):3146–3151. https://doi.org/10.1002/adma.200701983
15. Pedrero M, Campuzano S, Pingarrón JM (2017) Electrochemical (bio)sensing of clinical markers using quantum dots. Electroanalysis 29(1):24–37. https://doi.org/10.1002/elan.201600547
16. Zheng XT, Ananthanarayanan A, Luo KQ, Chen P (2015) Glowing graphene quantum dots and carbon dots: properties, syntheses, and biological applications. Small 11(14):1620–1636. https://doi.org/10.1002/smll.201402648
17. Lin CH, Cheng B, Li TY, Retamal JRD, Wei TC, Fu HC, Fang X, He JH (2019) Orthogonal lithography for halide perovskite optoelectronic nanodevices. ACS Nano 13(2):1168–1176. https://doi.org/10.1021/acsnano.8b05859
18. Lin CH, Kang CY, Wu TZ, Tsai CL, Sher CW, Guan X, Lee PT, Wu T, Ho CH, Kuo HC, He JH (2020) Giant optical anisotropy of perovskite nanowire array films. Adv Funct Mater 30(14):1909275. https://doi.org/10.1002/adfm.201909275
19. Lin CH, Li TY, Zhang J, Chiao ZY, Wei PC, Fu HC, Hu L, Yu MJ, Ahmed GH, Guan X, Ho CH, Wu T, Ooi BS, Mohammed OF, Lu YJ, Fang X, He JH (2020) Designed growth and patterning of perovskite nanowires for lasing and wide color gamut phosphors with long-term stability. Nano Energy 73:104801. https://doi.org/10.1016/j.nanoen.2020.104801
20. Zhang Y, Li S, Yang W, Joshi MK, Fang X (2019) Millimeter-sized single-crystal $CsPbrB_3$/CuI heterojunction for high-performance self-powered photodetector. J Phys Chem Lett 10(10):2400–2407. https://doi.org/10.1021/acs.jpclett.9b00960

21. Jiaxin WY, Zhang CY, Zhang Y, He JH, Fang X (2019) Silicon-compatible photodetectors: trends to monolithically integrate photosensors with chip technology. Adv Funct Mater 29(18):1808182. https://doi.org/10.1002/adfm.201808182
22. Liu WW, Wu TH, Liu MC, Niu WJ, Chueh YL (2019) Recent challenges in perovskite solar cells toward enhanced stability, less toxicity, and large-area mass production. Adv Mater Interface 6(9):1801758. https://doi.org/10.1002/admi.201801758
23. Liu Z, Lin CH, Hyun BR, Sher CW, Lv Z, Luo B, Jiang F, Wu T, Ho CH, Kuo HC, He JH (2020) Micro-light-emitting diodes with quantum dots in display technology. Light Sci Appl 9:83. https://doi.org/10.1038/s41377-020-0268-1
24. Divitini G, Cacovich S, Matteocci F, Cina L, Di Carlo A, Ducati C (2016) In situ observation of heat-induced degradation of perovskite solar cells. Nat Energy 1(2):15012. https://doi.org/10.1038/nenergy.2015.12
25. Sun Q, Yin WJ (2017) Thermodynamic stability trend of cubic perovskites. J Am Chem Soc 139(42):14905–14908. https://doi.org/10.1021/jacs.7b09379
26. Liang J, Liu J, Jin Z (2017) All-inorganic halide perovskites for optoelectronics: progress and prospects. Solar RRL 1(10):1700086. https://doi.org/10.1002/solr.201700086
27. Calisi N, Caporali S, Milanesi A, Innocenti M, Salvietti E, Bardi U (2018) Composition dependent degradation of hybrid and inorganic lead perovskites in ambient conditions. Top Catal 61:1201–1208. https://doi.org/10.1007/s11244-018-0922-5
28. Protesescu L, Yakunin S, Bodnarchuk MI, Krieg F, Caputo R, Hendon CH, Yang RX, Walsh A, Kovalenko MV (2015) Nanocrystals of cesium lead halide perovskites ($CsPbX_3$, X = Cl, Br, and I): novel optoelectronic materials showing bright emission with wide color gamut. Nano Lett 15(6):3692–3696. https://doi.org/10.1021/nl5048779
29. Tien CH, Chen LC, Lee KY, Tseng ZL, Dong YS, Lin ZJ (2019) High-quality all-inorganic perovskite $CsPbBr_3$ quantum dots emitter prepared by a simple purified method and applications of light-emitting diodes. Energies 12(18):3507. https://doi.org/10.3390/en12183507
30. Li Y, Wang X, Xue W, Wang W, Zhu W, Zhao L (2019) Highly luminescent and stable $CsPbBr_3$ perovskite quantum dots modified by phosphine ligands. Nano Res 12(4):785–789. https://doi.org/10.1007/s12274-019-2289-8
31. Wang HC, Lin SY, Tang AC, Singh BP, Tong HC, Chen CY, Lee YC, Tsai TL, Liu RS (2016) Mesoporous silica particles integrated with all inorganic $CsPbBr_3$ perovskite quantum-dot nanocomposites (MP-PQDs) with high stability and wide color gamut used for backlight display. Angew Chem 55(28):7924–7929. https://doi.org/10.1002/anie.201603698
32. Yang C, Zhuang B, Lin J, Wang S, Liu M, Jiang N, Chen D (2020) Ultrastable glass-protected all-inorganic perovskite quantum dots with finely tunable green emissions for approaching Rec. 2020 backlit display. Chem Eng J 398:125616. https://doi.org/10.1016/j.cej.2020.125616
33. Wang S, Bi C, Yuan J, Zhang L, Tian J (2018) Original core–shell structure of cubic CsPbBr 3@amorphous $CsPbBr_x$ perovskite quantum dots with a high blue photoluminescence quantum yield of over 80%. ACS Energy Lett 3(1):245–251. https://doi.org/10.1021/acsenergylett.7b01243
34. Chen LY, Chen SH, Dai SJ, Kuo CT, Wang HC (2014) Spectral design and evaluation of OLEDs as light sources. Org Electron 15(10):2194–2209. https://doi.org/10.1016/j.orgel.2014.06.009
35. Tress W, Domanski K, Carlsen B, Agarwalla A, Alharbi EA, Graetzel M, Hagfeldt A (2019) Performance of perovskite solar cells under simulated temperature-illumination real-world operating conditions. Nat Energy 4:568–574. https://doi.org/10.1038/s41560-019-0400-8
36. Bi K, Wang D, Wang P, Duan B, Zhang T, Wang Y, Zhang H, Zhang Y (2017) Cesium lead halide perovskite quantum dot-based warm white light-emitting diodes with high color rendering index. J Nanopart Res 19:174. https://doi.org/10.1007/s11051-017-3862-2
37. Wu Z, Wei J, Sun Y, Wu J, Hou Y, Wang P, Wang N, Zhao Z (2019) Air-stable all-inorganic perovskite quantum dot inks for multicolor patterns and white LEDs. J Mater Sci 54:6917–6929. https://doi.org/10.1007/s10853-019-03382-2
38. Xie Y, Yu Y, Gong J, Yang C, Zeng P, Dong Y, Yang B, Liang R, Ou Q, Zhang S (2018) Encapsulated room-temperature synthesized $CsPbX_3$ perovskite quantum dots with high stability and wide color gamut for display. Opt Mater Express 8(11):3494–3505. https://doi.org/10.1364/OME.8.003494
39. Lee MJ, Lee J, Yang HS, Hong KS (2017) Emission of CdSe quantum dots according to the capping ligands. Curr Appl Phys 17(6):880–884. https://doi.org/10.1016/j.cap.2017.03.008
40. Dai S, Siao CB, Chung SR, Wang KW, Pan X (2018) Developed one-pot synthesis of dual-color CdSe quantum dots for white light-emitting diode application. J Mater Chem C 6(12):3089–3096. https://doi.org/10.1039/C8TC00348C
41. Qian G, Lin Y, Wantz G, Davis AR, Carter KR, Watkins JJ (2014) Saturated and multi-colored electroluminescence from quantum dots based light emitting electrochemical cells. Adv Funct Mater 24(28):4484–4490. https://doi.org/10.1002/adfm.201400167
42. Manna L, Scher EC, Alivisatos AP (2000) Synthesis of soluble and processable rod-, arrow-, teardrop-, and tetrapod-shaped CdSe nanocrystals. J Am Chem Soc 122(51):12700–12706. https://doi.org/10.1021/ja003055+
43. Zhang Q, Joo JB, Lu Z, Dahl M, Oliveira DQL, Ye M, Yin Y (2011) Self-assembly and photocatalysis of mesoporous TiO_2 nanocrystal clusters. Nano Res 4:103–114. https://doi.org/10.1007/s12274-010-0058-9
44. Talapin DV, Rogach AL, Kornowski A, Haase M, Weller H (2001) Highly luminescent monodisperse CdSe and CdSe/ZnS nanocrystals synthesized in a hexadecylamine–trioctylphosphine oxide–trioctylphospine mixture. Nano Lett 1(4):207–211. https://doi.org/10.1021/nl0155126
45. Wu L, Zhong Q, Yang D, Chen M, Hu H, Pan Q, Liu H, Cao M, Xu Y, Sun B, Zhang Q (2017) Improving the stability and size tunability of cesium lead halide perovskite nanocrystals using trioctylphosphine oxide as the capping ligand. Langmuir 33(44):12689–12696. https://doi.org/10.1021/acs.langmuir.7b02963
46. Huang G, Li F, Cai Z, Zhang M (2019) Synthesis of highly luminescent $CsPb_xMn_{1-x}Cl_3$ perovskite nanocrystals via using metal–organic Mn-complex as precursor. J Alloys Compd 791:621–627. https://doi.org/10.1016/j.jallcom.2019.03.353
47. Liu F, Zhang YH, Ding C, Kobayashi S, Izuishi T, Nakazawa N, Toyoda T, Ohta T, Hayase S, Minemoto T, Yoshino K, Dai S, Shen Q (2017) Highly luminescent phase-stable $CsPbI_3$ perovskite quantum dots achieving near 100% absolute photoluminescence quantum yield. ACS Nano 11(10):10373–10383. https://doi.org/10.1021/acsnano.7b05442
48. Koolyk M, Amgar D, Aharona S, Etgar L (2016) Kinetics of cesium lead halide perovskite nanoparticle growth: focusing and de-focusing of size distribution. Nanoscale 8(12):6403–6409. https://doi.org/10.1039/C5NR09127F

Publisher's Note